Low-loss amorphous silicon waveguides grown by PECVD on indium tin oxide

Sandro Rao
sandro.rao@unirc.it

Department of Information Science, Mathematics, Electronics and Transportations (DIMET)
"Mediterranea" University, Via Graziella Località Feo di Vito, Reggio Calabria, 89060, Italy

Francesco G. Della Corte

Department of Information Science, Mathematics, Electronics and Transportations (DIMET)
"Mediterranea" University, Via Graziella Località Feo di Vito, Reggio Calabria, 89060, Italy

Caterina Summonte

Institute for Microelectronics and Microsystems, Consiglio Nazionale delle Ricerche -
Unit of Bologna, Via Gobetti 101, Bologna, 40129, Italy

Low-loss hydrogenated amorphous silicon (α-Si:H) waveguides were realized by plasma enhanced chemical vapour deposition (PECVD) on a transparent conductive oxide (TCO) layer which is intended to provide the buried contact for the application of an external bias in active devices, e.g. switches and modulators. In particular we propose a technological solution to overcome both the strong reduction in optical transmittance due to the very high extinction coefficient of metal contacts and, at the same time, the optical scattering induced by the texturization effect induced in α-Si:H films grown on TCO. The very high optical propagation losses were minimized by depositing a spin-on-glass (SOG) layer between the α-Si:H core-layer and the TCO bottom contact. In this case, propagation losses of 2.5 dB/cm at 1550 nm were measured. All the fabricated samples were optically characterized and the surface roughness was accurately measured using a mechanical profilometer. We observed that, for an α-Si:H core-layer directly deposited on the TCO contact, the surface roughness is of the order of 100 nm leading to totally opaque waveguides. The experimental performances have been compared to those obtained through calculations using an optical simulation package. The results are found to be in agreement with the experimental data. [DOI: 10.2971/jeos.2010.10039s]

Keywords: amorphous silicon, waveguides, plasma enhanced chemical vapour deposition, transparent conductive oxide, spin on glass

1 INTRODUCTION

Crystalline silicon waveguides and photonics devices based on SOI technology have been an active field of research for more than 10 years [1]. Compared to III/V-compound semiconductors, an inherent advantage of this material is the cost and simplicity of processing. The demand for high refractive-index differences in order to create photonic crystals or high-speed optical modulators [2] have driven these efforts.

For the fabrication of active devices, like switches and modulators, two or more electrical contacts have to be embedded inside the structure to allow the application of an external bias. Although standard microelectronic processes provide plenty of technologies for the formation of metal contacts, their deployment has in general a negative impact on the optical characteristics of the devices, especially in terms of propagation losses. The preferred solution in these cases consists in adopting either highly doped (poly-) silicon layers [2, 3], or a transparent conductive oxide (TCO), like Indium Tin Oxide (ITO) or Tin Oxide (TO) [4]–[8]. These last materials, widely deployed in thin film solar cell technology [9], offer some advantages over doped silicon in terms of electrical properties, with a conductivity which can be as high as 1.8×10^3 Ωcm^{-1} [10, 11], and optical properties, with a refractive index n as low as 0.5 at 1500 nm wavelength [12], therefore ensuring the high refractive-index difference required in sub-micron waveguiding devices.

Unfortunately, TCO films can only be used for top contacts, because the SOI technology does not allow laying it at the waveguide bottom, i.e. between the SiO$_2$ cladding and the silicon core. Therefore only highly doped silicon films can be used in this case [2, 3].

With the recently growing interest for hydrogenated amorphous silicon (α-Si:H) deposited at relatively low temperatures ($T < 300°$) as a suitable material for integrated passive [13]–[17] and active [8, 18, 19] photonic devices, and the consequent reduction of the thermal budged required for their fabrication, many otherwise unusable materials and technologies might gain a role in this field. ITO, in particular, can be considered a valid candidate for a simple formation of the buried contacts in multi-layer devices. Unfortunately, some drawbacks might derive in this case from the very high extinction coefficient of ITO ($k = 0.6$ at $\lambda = 1.55$ μm [12]), whose negative consequences are enhanced by the known texturization effect observed in the α-Si:H films grown on TCO [20, 21]. In fact, for the extreme light confinement in submicron strip waveguides, propagation losses due to the interaction of the waveguiding modes with the interface roughness are significantly increased and can become prohibitive for dense integrated circuits [22, 23].

In this paper we report technological results and compare the loss measurements concerning α-Si:H waveguides, either di-

	Stack		
Layer	**1**	**2**	**3**
SiO_2 /nm	310	310	310
ITO /nm	80	80	-
SOG /nm	160	-	-
α-Si:H /nm	1440	1590	1440

TABLE 1 Layer thicknesses for the three realized multistack waveguides.

FIG. 1 Specular reflectance of stacks 1 and 2. Bold lines: experimental data. Thin lines: computed data.

rectly deposited on ITO, or separated from this by a thin spin-on-glass (SOG) layer.

The experimental performances have been compared to those obtained through calculations using an optical simulation package. The results are found to be in agreement with the experimental data.

2 WAVEGUIDE FABRICATION

In an active α-Si:H-based photonic device, thin films of this semiconductor may be deposited on top of an ITO layer in a RF or DC glow-discharge plasma of SiH_4, pure or mixed with other gases. At the time of the deposition of the first α-Si:H layer, the ITO film is primarily exposed to a plasma hydrogen containing. This results in a degradation of the TCO caused by the reduction of the oxide surface to the corresponding elemental metals [21].

As a consequence, a memory of the surface roughness of the ITO substrate is retained in the growing α-Si:H film [24]. It should be mentioned that this effect is somehow useful in thin film solar cells because it helps improving their efficiency by favouring light trapping [25].

On the other hand, this behaviour leads to serious problems in waveguiding photonic devices, and primarily to high transparency loss in the interface region of the amorphous silicon films at the IR wavelengths. Moreover, TCO films deposited on α-Si:H show an increasing roughness with the deposition temperature [11].

The impact of the ITO film morphology on the propagation losses in α-Si:H-based waveguides, and a new technological solution to overcome this issue are outlined in the following. In particular, the α-Si:H was uncoupled from the ITO surface by inserting a SOG layer in between. Three waveguides were realized. For all samples, the substrate is a doped c-Si wafer ($\rho = 0.001$ Ωcm) and the waveguide core is about 1.5 μm-thick α-Si:H layer. The substrate and the stack are separated by a 310 nm-thick low refractive index LPCVD SiO_2 cladding layer, so that a good vertical confinement is achieved.

The geometrical data of the waveguides are summarised in Table 1.

The fabrication of the first waveguide begins with a surface cleaning treatment, using H_2SO_4 + H_2O_2 and HF solution on the n-type doped c-Si substrate. The substrate was than loaded into the four-chamber RF (13.56 MHz) system.
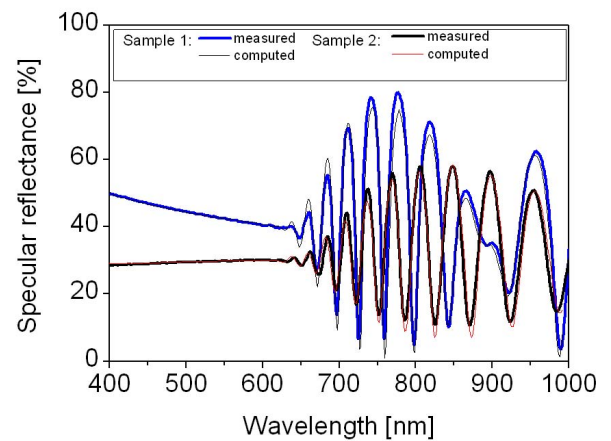
The SiO_2 cladding layer was grown by wet thermal oxidation. Subsequently the 80 nm-thick ITO layer was deposited by RF magnetron sputtering using a In_2O_3:SnO_2 ceramic target, at 250°C substrate temperature and a base pressure adjusted to 10^{-5} torr [26]. The SOG spinning on the ITO layer was done at 4000 rpm, followed by three pre-baking steps of 60 s each, at 80°C, 150°C, and 200°C respectively, and a furnace annealing at 425°C for 30 min in flowing nitrogen. Finally the α-Si:H layer was deposited in SiH_4 atmosphere by an RF Plasma Enhanced Chemical Vapour deposition (PECVD) at the frequency of 13.56 MHz, 220°C substrate temperature, 0.55 mbar gas pressure and 20 sccm (standard cubic centimetres per minute) silane flow rate. The base vacuum was 4×10^{-8} mbar. The deposition time was adjusted to obtain films thickness of about 1.5 μm. The fabrication of the second and third waveguides followed the same procedure, although SOG and ITO/SOG layer depositions were skipped for sample 2 and sample 3 respectively.

Note that in sample 1 the active α-Si:H layer is indeed insulated from the buried ITO contact. However, this is not really a problem, as small via-holes can be locally introduced across the SOG layer, e.g. laterally to the waveguide core, for warranting electrical continuity between the buried contact and the active device.

3 MEASUREMENTS

3.1 Optical Characterization

The samples were optically characterized using specular spectral reflectance R. Data were obtained using an optical fiber UV-visible spectrophotometer (Avantes). Figure 1 shows the experimental and computed R spectra for samples 1 and 2.

For both samples, at wavelengths longer than 650 nm, an interference pattern is visible, which reflects the contribution of all interfaces down to the silicon surface. For shorter wavelengths, no fringe pattern is visible. In fact, due to film absorption, there is no contribution to R coming from the interface of α-Si:H with SOG. In other words, the α-Si:H film behaves as a bulk. Therefore, the R curves should coincide for
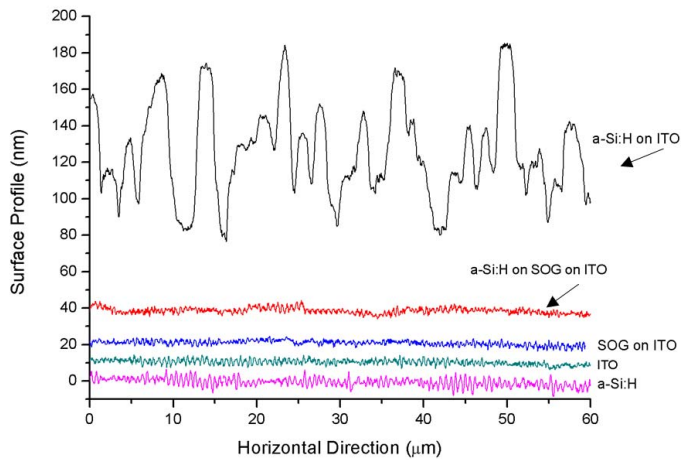
FIG. 2 Surface roughness profile for the different samples. The curves were vertically shifted for clarity. The vertical shift is not related to film thickness.

the two samples. Yet, for sample 2 a severe damping of the signal, stronger at shorter wavelengths, is observed. This indicates the presence of roughness at the α-Si:H surface, that causes light scattering and consequent decrease of the specularly reflected light intensity.

Simulations were obtained using the OPTICAL computer code, which makes use of a Generalized Scattering Matrix Method to treat multilayers with any distribution of coherent or incoherent behaviour [27], associated to χ^2 minimization. The simulation of sample 1 was performed using flat surfaces (thin black line in Figure 1), while simulation of sample 2 required the introduction of 25 nm roughness at the α-Si:H surface. The roughness was accounted for by using modified Fresnel coefficients, according to the exponential decay model of the rough interface [28].

3.2 Mechanical profiling

The surface roughness was measured on all samples. Figure 2 shows the profiles taken using a mechanical profilometer (Veeco Dektak 6M). The curves where vertically shifted each other for the sake of clarity, the shift having no correlation with the actual film thickness. The roughness of amorphous silicon, when grown on top of ITO, is evident. In this case a statistic on surface profiling gives a standard deviation of ± 29 nm, which correlates very well with the value obtained by optical simulation. When a layer of SOG is inserted between the two, the roughness is greatly reduced. The roughness of ITO itself, SOG, and amorphous silicon deposited on SiO_2/c-Si is below the detection limit of this technique.

3.3 Waveguide characterization

Propagation loss measurements were made for the three different waveguides with the cut-back technique [29]. This method is based on measuring the light transmission through waveguides of different lengths and fitting the experimental data length dependence, assuming identical coupling conditions and constant facet quality.

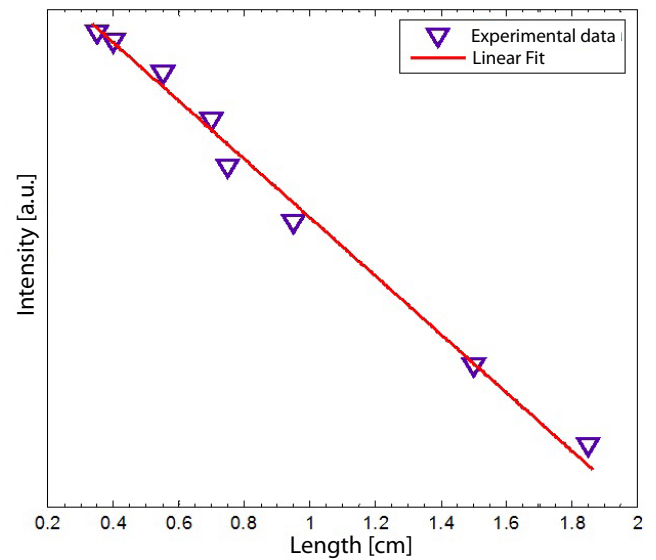In our experiments, the probe beam was a 15 mW laser diode

FIG. 3 Transmitted light intensity, though sample 1, vs. waveguide lengths (from 0.35 cm to 1.85 cm). The waveguide consists of the stack of α-Si:H (1.44 μm-thick) on SOG (160 nm-thick) on ITO (80 nm-thick).

	Stack		
	1	**2**	**3**
α [dB/cm] (Experimental)	2.5 ± 0.1	No transmission	1.5 ± 0.1
α [dB/cm] (Simulation TE)	1.8	32.1	1.1
α [dB/cm] (Simulation TM)	3.2	67.8	1.3

TABLE 2 Waveguide absorption coefficient at 1550 nm, measured and theoretical, for the different samples.

radiation ($\lambda = 1.55$ μm), coupled to the waveguide core via a 5 μm-core single-mode fiber, without polarization control. The transmitted light was collected at the chip output by a multimode fiber and detected by an InGaAs photodiode. Great care was taken to prevent stray light passing above the sample.

Several samples from different wafers with lengths up to 2 cm were cut by cleavage. Sample facets did not receive polishing treatment, although their good quality was verified by means of micro-optical inspections before measurements.

Figure 3 shows the measured transmitted power through type 1 waveguides with different lengths. The loss coefficient was extracted by linear regression. From the slope shown in the figure, we calculated an absorption coefficient of $\sim 2.5 \pm 0.1$ dB/cm at $\lambda = 1550$ nm. Note that this experimental attenuation for unpolarised light is intermediate between the theoretically estimated ones for the TE and TM modes, as reported in Table 2. The overall insertion losses are 10.4 dB, with the main contribution due to the coupling losses, a drawback of the high refractive index of silicon used as the core material.

Using the same technique, the loss coefficient of type 3 waveguide, consisting of the stack of 1.44 μm-thick α-Si:H on SiO$_2$, was measured to be $\sim$ 1.5 dB/cm, a value comparable to standard SOI waveguide losses in α-Si:H [15]. As the two devices differ only in the SOG/ITO layers of waveguide 1, we can conclude that this introduction is responsible for a loss increase of $\sim$ 1.0 dB/cm. It should be noted, finally, that the introduction of a bare ITO layer drove to totally opaque waveguides (type 2), due both to the high roughness of amorphous silicon grown on top of the ITO layer and its high extinction coefficient.

The experimental propagation losses are summarised in Table 2, which also lists the theoretical results, for both TE and TM polarizations, discussed in the next section.

3.4 Waveguide simulations and discussion

Figure 4 illustrates the schematic cross sections considered in this paper. The undoped α-Si:H layer, 1.44 μm-thick, is deposited either directly on the ITO thin layer (sample 2, see Figure 4(b)), or separated from this by a SOG layer (sample 1, see Figure 4(a)). In Figure 4(c) we report a standard SOI waveguide in α-Si:H on SiO$_2$ (sample 3).

Optical simulations were performed using Beamprop, the device simulation package from RSoft [30]. Most of the optical data of the materials used for simulations were determined from the analysis of the experimental transmittance and reflectance spectra, in the wavelength range 0.5 μm to 2 μm, of test films deposited on corning glass. The reflectance-transmittance analysis tool OPTICAL [27] was used for this analysis, which also allowed determining the layer thicknesses. Photothermal deflection spectroscopy (PDS) [31] was used to determine the absorption coefficient of α-Si:H at $\lambda = $ 1.55 μm. The material characteristics, at this wavelength, are listed in Table 3.

The waveguides have been designed in order to ensure only the propagation of the fundamental mode and for this purpose the optical mode spectrum was also modeled. The waveguide geometries were chosen according to [32], to satisfy the single mode condition. Simulations demonstrated that the designed waveguiding structures exhibit a dominant single-mode operation for TE and TM polarization modes once a 5 μm wide rib is defined by photolithographic patterning and etching process. The shallow etch depth is 60 nm. In Figure 5 we report the fundamental optical mode-field profiles of samples 1, 2, 3, for both, TE and TM polarizations.

We calculated the propagation losses for the three realized structures. The corresponding results, for both polarization conditions, are again reported in Table 2. Due to the presence of the lossy ITO thin layer in sample 1 and 2, the TM mode exhibits higher losses if compared to TE mode since part of the TM polarized light propagates into the underlying ITO layers.

Moreover, it should be noted that the simulated data of 32.1 dB/cm and 67.8 dB/cm were calculated without considering the interface roughness between ITO and α-Si:H.
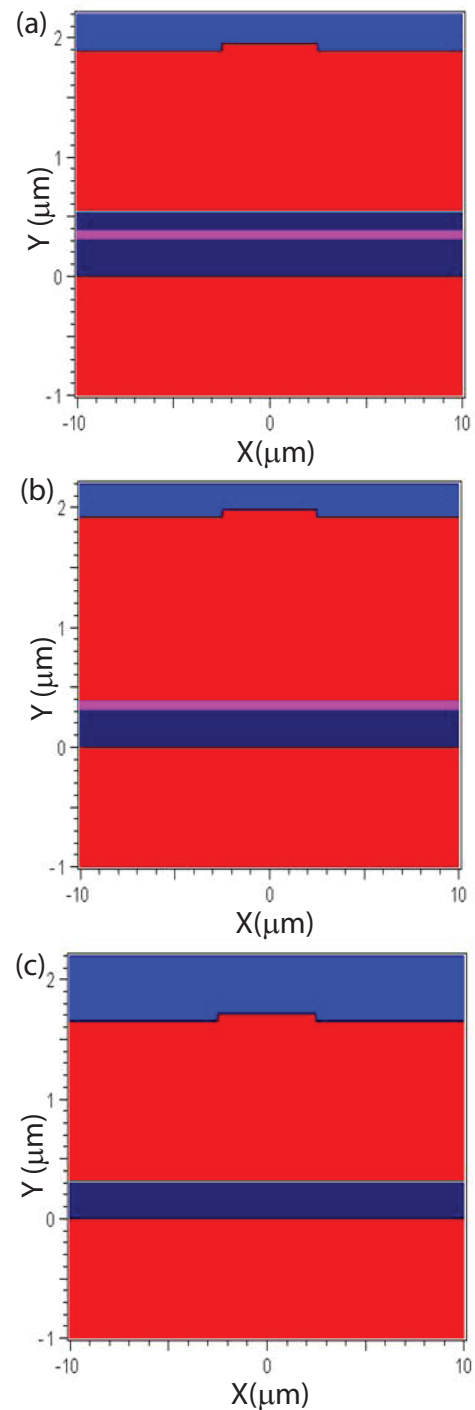

FIG. 4 Schematic cross section of the realized waveguides. The crystalline silicon substrate is 300 mm thick. a) sample 1, b) sample 2, and c) sample 3.

Material	n	k
SiO$_2$	1.45 ± 0.02	1.0×10^{-6}
ITO	0.5 ± 0.01	0.6
SOG	1.45	0
α-Si:H	3.58 ± 0.02	3.0×10^{-6}

TABLE 3 Refractive index n, and extinction coefficient k, measured at 1.55 μm.

These results allow to conclude that the optical propagation in the waveguides with no interface roughness between the buried ITO contact and the α-Si:H waveguide core is also limited by the ITO absorption. As a consequence, an optimum

(a) Computed Transverse Mode Profile (m = 0, n_{eff} = (3.508597))

(b) Computed Transverse Mode Profile (m = 0, n_{eff} = (3.493724))

(c) Computed Transverse Mode Profile (m = 0, n_{eff} = (3.507928))

(d) Computed Transverse Mode Profile (m = 0, n_{eff} = (3.492221))

(e) Computed Transverse Mode Profile (m = 0, n_{eff} = (3.508843))

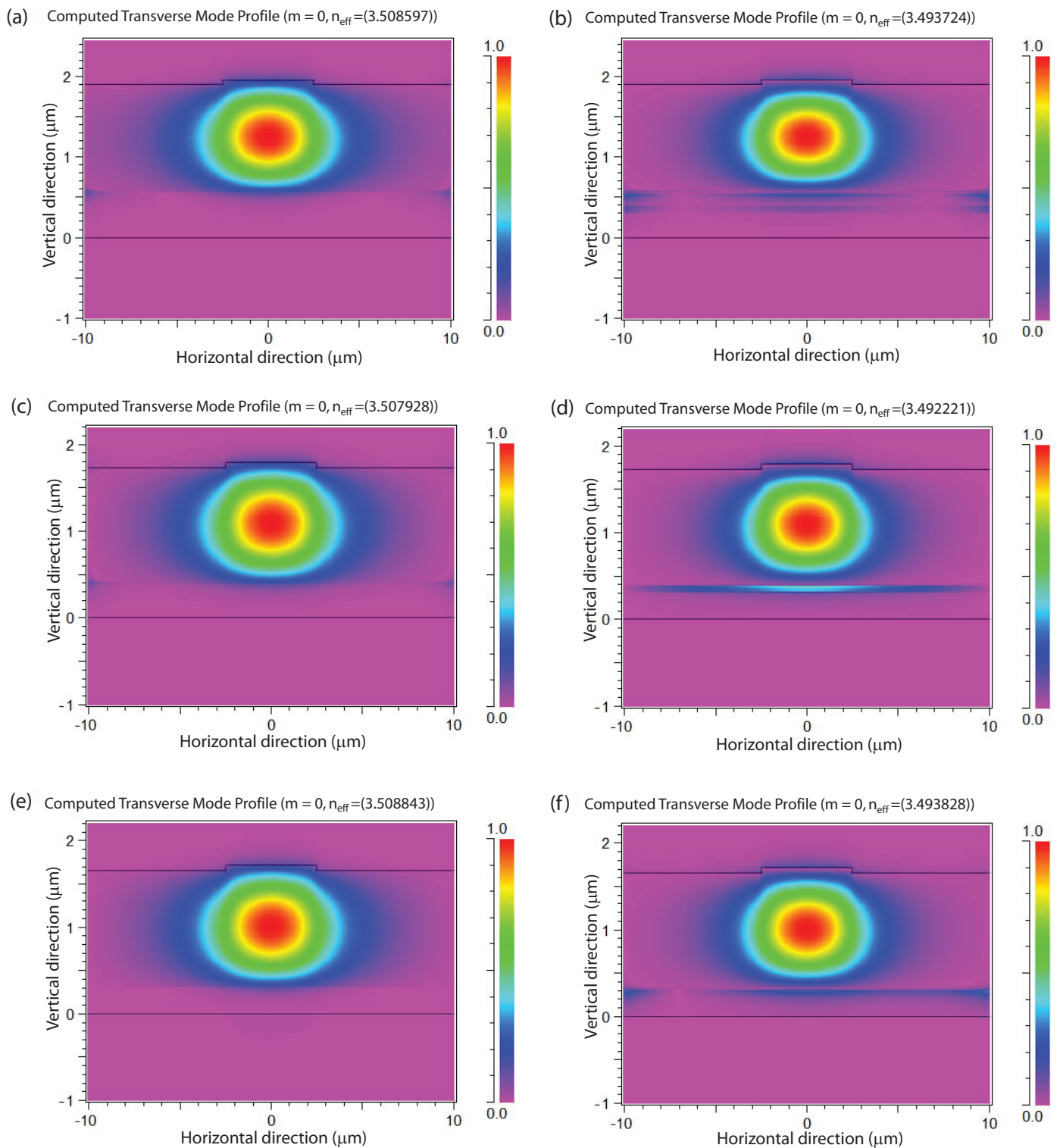(f) Computed Transverse Mode Profile (m = 0, n_{eff} = (3.493828))

FIG. 5 TE (a, c, e) and TM (b, d, f) fundamental optical mode-field profiles of samples 1, 2, 3, respectively.

design of the structure and a careful control of the light signal confinement inside the α-Si:H core layer would permit the realization of waveguides with losses lower than 1.5 dB/cm, which is considered a sort of threshold for integrated optic links [33].

For this purpose we simulated a new waveguide which differs from sample 1 only in the SOG thickness. If we consider a SOG thickness of 210 nm, instead of 160 nm, the waveguide

propagation losses, for the TE mode, decrease from 1.8 dB/cm to 1.1 dB/cm, which is equal to that estimated for sample 3.

4 CONCLUSIONS

The negative impact of a buried transparent conductive oxide layer on the propagation losses in α-Si:H-based waveguides, grown on an ITO layer useful as a buried contact, was studied. All the fabricated samples were optically characterized

and the surface roughness was accurately measured using a mechanical profilometer. We observed that, for an α-Si:H core-layer directly deposited on ITO, the surface roughness, due to the interaction of ITO with hydrogen during the PECVD deposition, is of the order of 100 nm. This leads to prohibitive propagation losses for the waveguide, which on the other hand drop to 1.5 dB/cm in waveguides not including the ITO buried layer. The strong reduction in the optical transmittance was recovered by depositing a spin-on-glass layer between the 1.44 μm-tick α-Si:H core-layer and the ITO layer. In this case, propagation losses of 2.5 dB/cm at 1550 nm were measured.

The experimental results have been compared to those obtained through calculations using an optical simulation package. The results were found to be in agreement with the experimental data.

Technologically, the waveguide fabrication process involves temperatures lower than 450°C, which are compatible with standard microelectronic processes and in particular suitable for the realization of a photonic layer on top of an integrated circuit.

ACKNOWLEDGMENTS

References

[1] G. T. Reed, and A. P. Knights, *Silicon Photonics: An Introduction* (John Wiley & Sons, New York, 2004).

[2] A. Liu, R. Jones, L. Liao, D. Samara-Rubio, D. Rubin, O. Cohen, R. Nicolaescu, and M. Paniccia, "A high-speed optical modulator based on a metal-oxide-semiconductor capacitor" Nature **427**, 615–618 (2004).

[3] D. Marris-Morini, X. Le Roux, L. Vivien, E. Cassan, D. Pascal, M. Halbwax, S. Maine, S. Laval, J. M. Fédéli, and J. F. Damlencourt, "Optical modulation by carrier depletion in a silicon PIN diode" Opt. Express **14**, 10838–10843 (2006).

[4] S. M. Weiss, H. Ouyang, J. Zhang, and P. M. Fauchet, "Electrical and thermal modulation of silicon photonic bandgap microcavities containing liquid crystals" Opt. Express **13**, 1090–1097 (2005).

[5] S. E. Holland, N. W. Wang, and W. W. Moses, "Development of low noise, back-side illuminated silicon photodiode arrays" IEEE T. Nucl. Sci. **44**, 443–447 (1997).

[6] B. Shi, P. S. Chang, K. Sun, Y. Xie, C. Radhakrishnan, and H. G. Monbouquette, "Monolithic integrated modulator on silicon for optical interconnects" IEEE Photonic. Tech. L. **19**, 55–57 (2007).

[7] J. F. Du, X. F. Gu, X. F. Huang, J. Zhou, K. J. Chen, H. Chen, J. H. Yang, and B. C. Cao, "Hydrogenated amorphous silicon PIN photodiode for optically addressed spatial light modulators" in *Proceedings to the 4th International Solid-State and Integrated Circuit Technology*, 733–735 (IEEE, Beijing, 1995).

[8] F. G. Della Corte, S. Rao, M. A. Nigro, F. Suriano, and C. Summonte, "Electro-optically induced absorption in α-Si:H/α-SiCN waveguiding multistacks" Opt. Express **16**, 7540–7550 (2008).

[9] M. A. Green, "Thin-film solar cells: review of materials, technologies and commercial status" J. Mater. Sci. **18**, 15–19 (2007).

[10] B. G. Lewis, and D. C. Paine, "Applications and processing of transparent conducting oxides" MRS Bull. **25**, 22–27 (2000).

[11] S. Diplas, A. Ulyashin, K. Maknys, A. E. Gunnaes, S. Jørgensen, D. Wright, J. F. Watts, A. Olsen, and T. G. Finstad, "On the processing–structure–property relationship of ITO layers deposited on crystalline and amorphous Si" Thin Solid Films **515**, 8539–8543 (2007).

[12] R. A. Synowicki, "Spectroscopic ellipsometry characterization of indium tin oxide film microstructure and optical constants" Thin Solid Films **313**, 394–397 (1998).

[13] G. Cocorullo, F. G. Della Corte, R. De Rosa, I. Rendina, A. Rubino, and E. Terzini, "Amorphous silicon-based guided-wave passive and active devices for silicon integrated optoelectronics" IEEE J. Sel. Top. Quant. **4**, 997–1002 (1998).

[14] S. K. Selvaraja, E. Sleeck, M. Schaekers, W. Bogaerts, D. V. Thourhout, P. Dumon, and R. Baets, "Low-loss amorphous silicon-on-insulator technology for photonic integrated circuitry" Opt. Commun. **282**, 1767–1770 (2009).

[15] A. Harke, M. Krause, and J. Mueller, "Low-loss singlemode amorphous silicon waveguides" Electron. Lett. **41**, 1377–1379 (2005).

[16] M. J. A. de Dood, A. Polman, T. Zijlstra, and E. W. J. M. van der Drift, "Amorphous silicon waveguides for microphotonics" J. Appl. Phys. **92**, 649–653 (2002).

[17] J. M. Fedeli, L. Di Cioccio, D. Marris-Morini, L. Vivien, R. Orobtchouk, P. Rojo-Romeo, C. Seassald, and F. Mandorlo, "Development of silicon photonics devices using microelectronic tools for the integration on top of a CMOS wafer" Adv. Opt. Technol. **2008**, 412518 (2008).

[18] G. Cocorullo, F. G. Della Corte, R. De Rosa, I. Rendina, C. Minarini, A. Rubino, and E. Terzini, "Amorphous silicon waveguides and light modulators for integrated photonics realized by low-temperature plasma enhanced chemical-vapor deposition" Opt. Lett. **21**, 2002–2004 (1996).

[19] M. Iodice, G. Mazzi, and L. Sirleto, "Thermo-optical static and dynamic analysis of a digital optical switch based on amorphous silicon waveguide" Opt. Express **14**, 5266–5278 (2006).

[20] J. Lan, and J. Kanicki, "ITO surface ball formation induced by atomic hydrogen in PECVD and HW-CVD tools" Thin Solid Films **304**, 123–129 (1997).

[21] R. Banerjee, S. Ray, N. Basu, A. K. Batabyal, and A. K. Barua, "Degradation of tin-doped indium-oxide film in hydrogen and argon plasma" J. Appl. Phys. **62**, 912–916 (1987).

[22] K. K. Lee, D. R. Lim, and L. C. Kimerling, "Fabrication of ultralow-loss Si/SiO waveguides by roughness reduction" Opt. Lett. **26**, 1888–1890 (2001).

[23] P. Dumon, W. Bogaerts, J. van Campenhout, V. Wiaux, J. Wouters, S. Beckx, and R. Baets, "Low-loss photonic wires and compact ring resonators in silicon-on-insulator" in *Proceedings to 2003 IEEE/LEOS Symposium Benelux Chapter*, 5–8 (IEEE, Twente, 2003).

[24] S. Kumar, and B. Drevillon, "A real time ellipsometry study of the growth of amorphous silicon on transparent conducting oxides" J. Appl. Physics **65**, 3023–3034 (1989).

[25] L. Meng, A. Maqarico, and R. Martins, "Study of annealed indium tin oxide films prepared by RF reactive magnetron sputtering"

Vacuum **46,** 673–680 (1995).

[26] M. G. Zebaze Kana, E. Centurioni, D. Iencinella, and C. Summonte, "Influence of the sputtering system's vacuum level on the properties of indium tin oxide films" Thin Solid Films **500,** 203–208 (2006).

[27] E. Centurioni, "Generalized matrix method for calculation of internal light energy flux in mixed coherent and incoherent multilayers" Appl. Opt. **44,** 7532–7539 (2005).

[28] D. G. Stearns, D. P. Gaines, and D. W. Sweeney, "Nonspecular x-ray scattering in a multilayer-coated imaging system" J. Appl. Phys **84,** 1003–1028 (1998).

[29] G. Cancellieri, and U. Ravaioli, *Measurements of Optical Fibers and Devices: Theory and Experiments* (Artech House, Dedham, 1984).

[30] *RSoft Photonics CAD Layout User Guide* (RSoft Design Group, Ossining).

[31] W. B. Jackson, N. M. Amer, A. C. Boccara, and D. Fournier, "Photothermal deflection spectroscopy and detection" Appl. Opt. **20,** 1333–1344 (1981).

[32] S. P. Chan, C. E. Png, S. T. Lim, G. T. Reed, and V. M. N. Passaro, "Single-mode and polarization-independent silicon-on-insulator waveguides with small cross section" J. Lightwave Technol. **23,** 2103–2111 (2005).

[33] R. A. Soref, "Silicon-based optoelectronics" P. IEEE **81,** 1687–1706 (1993).